Combustion Science and Technology

Publication details, including instructions for authors and subscription information:
http://www.tandfonline.com/loi/gcst20

STRUCTURE AND DYNAMICS OF CRYOGENIC FLAMES AT SUPERCRITICAL PRESSURE

S. CANDEL* [a], M. JUNIPER† [a], G. SINGLA [a], P. SCOUFLAIRE [a] & C. ROLON [a]

[a] EM2C Laboratory, CNRS, Ecole Centrale Paris, France

Available online: 25 Jan 2007

To cite this article: S. CANDEL*, M. JUNIPER†, G. SINGLA, P. SCOUFLAIRE & C. ROLON (2006): STRUCTURE AND DYNAMICS OF CRYOGENIC FLAMES AT SUPERCRITICAL PRESSURE, Combustion Science and Technology, 178:1-3, 161-192

To link to this article: http://dx.doi.org/10.1080/00102200500292530

Combust. Sci. and Tech., 178: 161–192, 2006

ISSN: 0010-2202 print/1563-521X online
DOI: 10.1080/00102200500292530

Taylor & Francis
Taylor & Francis Group

STRUCTURE AND DYNAMICS OF CRYOGENIC FLAMES AT SUPERCRITICAL PRESSURE

S. CANDEL*
M. JUNIPER†
G. SINGLA
P. SCOUFLAIRE
C. ROLON

EM2C Laboratory, CNRS, Ecole Centrale Paris, France

A detailed understanding of liquid propellant combustion is necessary for the development of improved and more reliable propulsion systems. This article describes experimental investigations aimed at providing such a fundamental basis for design and engineering of combustion components. It reports recent applications of imaging techniques to cryogenic combustion at high pressure. The flame structure is investigated in the transcritical range where the pressure exceeds the critical pressure of oxygen ($p > p_c(O_2 = 5.04\,\mathrm{MPa})$) but the temperature of the injected liquid oxygen is below its critical value ($T_{O_2} < T_c(O_2) = 154\,\mathrm{K}$). Data obtained from imaging of OH^* radicals emission, CH^* radicals emission in the case of LOx/GCH_4 flames and backlighting provide a detailed view of the flame structure for a set of injection conditions. The data may be used to guide numerical modelling of transcritical flames and the theoretical and numerical analysis of the stabilization process. Calculations of the flame edge are used to illustrate this aspect. Results obtained may also be employed to devise engineering modelling tools and

Received 23 July 2004; accepted 26 May 2005.

We wish to thank CNES, Snecma and CNRS for their continuous support of our work in rocket propulsion. The assistance of the "Mascotte" team of Onera under the leadership of Lucien Vingert and Mohamed Habiballah is gratefully acknowledged.

***Also with Institut Universitaire de France.**

†**Present Address: Engineering Department, Cambridge University.**

Address correspondence to candel@em2c.ecp.fr

methodologies for component development aimed at improved efficiency and augmented reliability.

Keywords: cryogenic combustion, flame stabilization, transcritical injection

INTRODUCTION

Progress in liquid rocket propulsion technology during the second half of the 20th century has allowed extensive commercial utilization of space and a continuous growth of the launching market for telecommunications and earth observation satellites. Developments in space transportation systems have initially relied on accumulated experience from full scale testing, engineering analysis and application of basic combustion principles. In this context, research carried out during the last fifteen years has brought new insights on the processes controlling combustion in high performance rocket motors. Detailed experiments have provided a stream of data allowing design improvement and optimization. The data have been used to assist modelling efforts and validate numerical simulation tools. These, in turn, will allow a renewal of design methodologies for improving engine components and augmenting their service life.

Cryogenic combustion investigations described in this article are concerned with physical processes occurring in high-pressure chambers. The research effort focuses on combustion of liquid propellants, which are stored at low temperatures and require an external ignition to initiate the chemical reaction. Cryogenic reactants, such as liquid oxygen and hydrogen, are used in high performance propulsion systems. Examples include the Vulcain motor of the Ariane 5 first stage and the Space Shuttle main engines (SSME), which typically operate at pressures in excess of 10 MPa.

While early research into liquid rocket motors relied heavily on full scale testing with some model scale experiments but with limited diagnostic and data acquisition capabilities, the recent effort has exploited new model scale facilities and a set of optical and laser diagnostics to gather information on the process. The state of the art some 40 years ago is well synthesized in the textbook of Barrère et al. (1960). Systematic tests carried out on a wide variety of injection devices led to rapid adoption of certain injection configurations (Burick, 1972, 1973; Gill, 1978; Haarje and Reardon, 1972). These include coaxial injectors such as those represented schematically in Figure 1 that are generic and equip most

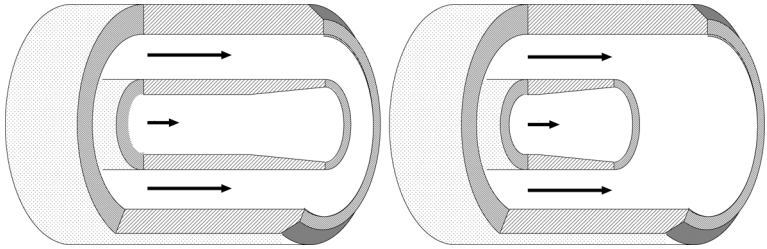

Figure 1. Coaxial injectors of the type used in rocket motors. Liquid oxygen flows through the central tube and gaseous hydrogen or methane through the annular passage. Left, the oxygen tube is set flush with the hydrogen channel. Right, the oxygen tube is recessed.

high-performance cryogenic engines. While the engineering know-how in practical design has become substantial as a result of successive developments and accumulation of test results, fundamental scientific questions relating to the physical processes at work in the chamber have remained unanswered until recently. These mainly relate to transients following ignition, flame propagation and spreading, the mechanism of flame stabilization, factors governing flame length and conversion efficiency, accurate estimation of heat transfer to the chamber walls and injection backplane, sensitivity to impulsive perturbations, combustion dynamics, and triggering of high frequency combustion instabilities.

An understanding of the flame structure is prerequisite to the solution of many technical problems. This question has been difficult to tackle because of the harsh conditions prevailing in the chamber and the difficulty of managing an optical access to the combustion region. Rocket engines release powers of several GW—the equivalent of a few large nuclear power plants—all within volumes of only a fraction of a cubic meter and at temperatures in excess of 3000 K. The power density reaches 50 to 100 $\mathrm{GW\,m^{-3}}$ while the chamber pressure is in the 10 to 20 MPa range. Even model scale testing is highly energetic and should be carried out at elevated pressures. Early experiments were also limited by sensor performance, data acquisition equipment, and processing devices. Much of the technological developments were therefore carried out without a detailed understanding of the parameters controlling the structure of the reactive flow and the dynamics of ignition and flame spreading during the engine start. While models or numerical simulation tools could not reproduce the complexity of the physical situation, engineering had to deal with many difficult problems including: (1) The definition of a

sequence ensuring a smooth ignition transient leading to a stable nominal operation; (2) The sizing of injection elements and thrust chamber providing the required efficiency; (3) Reduction of low frequency instabilities involving the feed line and chamber dynamics; and (4) Suppression of high frequency instabilities associated with the resonant coupling of combustion and chamber eigenmodes. Many spectacular failures were associated with dynamical phenomena and the related increase in heat transfer to the walls often leading to chamber burnout.

The scientific analysis of cryogenic combustion essentially began during the latter part of the twentieth century and these investigations have benefitted from advances in laser diagnostics, digital imaging cameras, experimental instrumentation, and high-speed digital data acquisition. Research facilities such as the University of Pennsylvania rocket propulsion test bed, Mascotte developed by Onera and P8 at DLR were made available during the same period and could be exploited for hot fire investigations under realistic injection conditions. In this general context, research has focused on the following items:

- Processes controlling liquid jet breakup, atomization, and mixing;
- Spray vaporization and combustion;
- Stabilization and flame spread near the injection backplane;
- Experimental diagnostics applicable to cryogenic flames under high-pressure conditions;
- Effect of pressure and transcritical phenomena.

Theoretical and numerical modelling efforts have also been carried out in parallel to integrate knowledge from experiments and advance engineering design methods.

This article reviews some of the more recent results of experimental investigations of high-pressure cryogenic combustion. Other data are available in the previous literature (see Candel et al., 1998; Herding et al., 1995, 1996, 1998; Juniper et al., 2000, 2001a, 2001b; Kendrick et al., 1998, 1999; Snyder et al., 1997; Tripathi, 2001) Another set of results are described in Mayer et al. (1996, 1998, 2000, 2001), and Mayer and Tamura (1996), but these studies pertain to a different range of injection conditions. Only imaging data are considered in what follows but there are some quantitative measurements of temperature and species (see e.g., Pal et al., 1996; Yeralan et al., 2001). Temperature measurements using Coherent Anti-Stokes Raman Scattering (CARS)

are discussed in a recent review by Candel et al. (2003) and in other contributions to the present issue.

Progress on the theoretical and numerical level has been achieved in parallel. A set of articles by Juniper et al. (2003), Juniper and Candel (2003a), Juniper and Candel (2003c) covers problems of flame stabilization. This has been approached by analyzing a series of generic problems that reveal the controlling parameters in carefully defined steps. Theoretical and numerical modelling has also been used to resolve some of the difficult questions raised by combustion of cryogenic propellants at high pressures by for example: Liang et al. (1985); Delplanque and Sirignano (1993a, 1993b); Daou et al. (1995); Oefelein and Yang (1998); Oefelein and Aggarwal (2000); Harstad and Bellan (2001); Okong'o et al. (2002); Okong'o and Bellan (2003); Jay et al. (2005); and the reviews by Yang (2000, 2004).

This article synthesizes information from imaging data and numerical modelling. It focuses on the following aspects: (a) high-pressure supercritical flame structure; (b) stabilization and flame spread in the nearfield, with emphasis on transcritical flames; (c) structure of transcritical LOx/methane flames; and (d) numerical modelling of flame stabilization. Next we describe some features of the Mascotte test facility. Flame structures are then discussed on the basis of emission imaging and backlighting. The injector nearfield is characterized with the same diagnostics. The main part of this article concerns LOx/GH_2 flames, but recent experiments carried out with LOx and gaseous methane (GCH_4) are also included in a separate section.

CRYOGENIC COMBUSTION FACILITY

Experiments described in this article were carried out at the Mascotte facility developed by ONERA to allow studies of elementary processes of atomization, vaporization, and turbulent combustion involved in cryogenic jet flames (Figure 2). The combustion chamber is equipped with a single-element injector fed with liquid oxygen (LOx) and gaseous hydrogen (GH_2). The injection head, holding the coaxial injector element, is cooled by liquid nitrogen (LN_2) to prevent heating of the LOx during injection. The injector element consists of a central tube fed with LOx surrounded by a parallel annular duct delivering gaseous hydrogen. (see Figure 1). Liquid oxygen is injected at a temperature of 85 K, while gaseous hydrogen is injected either at room temperature or may be

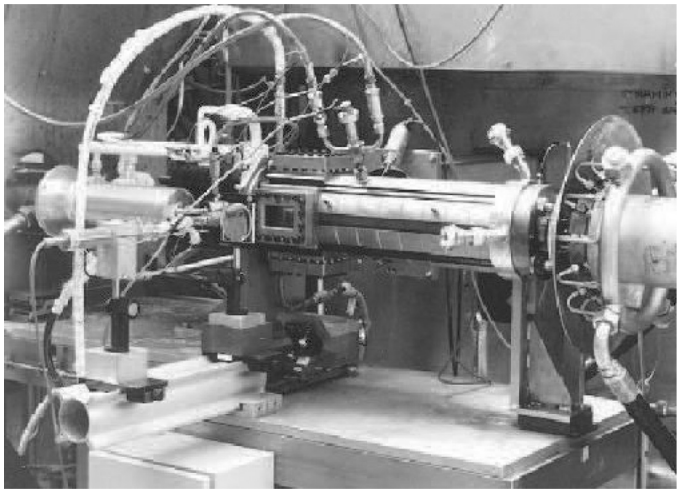

Figure 2. General view of the Mascotte combustor.

cooled down to a temperature of 100 K. In other experiments gaseous hydrogen is replaced by methane and this propellant is injected at room temperature. The test combustor can be operated up to pressures of 7 MPa, which exceeds the critical pressure of oxygen. The maximum LOx mass flow rate is 200 g s^{-1}, but most studies are carried out with mass flow rates of 50 or 100 g s^{-1}.

The combustion chamber itself is a square duct of 50 mm inner dimension made of stainless steel fitted with four fused silica windows for optical access. The two lateral windows are 100 mm long and 50 mm high. Their internal face is cooled by a gaseous helium film. The upper and lower windows are 100 mm long and 10 mm wide in early versions. In later versions they are 100 mm long and 50 mm wide. They may be used to transmit a longitudinal light sheet for laser imaging. The test section comprises interchangeable modules, allowing explorations of chamber sections located at various distances from the injection plane (the total chamber length is 425 mm). This is achieved by moving the visualization unit to different longitudinal positions. Interchangeable nozzles terminate the chamber and their throat diameter is selected to obtain the desired pressure. There is no water cooling and the chamber design, based on simplified thermomechanical models, allows 30 s of operation at atmospheric pressure, with a maximum mass flow rate of

120 g s^{-1} at a mixture ratio, $E = \dot{m}_{LOx}/\dot{m}_{GH_2}$, of 6. For oxygen/hydrogen combustion, the stoichiometric mass ratio is 8, hence hydrogen is in excess and the LOx mass flow rate determines the power. The test duration is reduced to 20 s at higher pressures. The combustor may be fired six to ten times a day, with 5 to 10 minutes between successive runs. Besides the mixture ratio, one important similarity parameter for the liquid jet breakup process, is the ratio of momentum fluxes at the injection plane defined as:

$$J = \frac{(\rho v^2)_{GH_2}}{(\rho v^2)_{LOx}} = \frac{\text{gas momentum flux}}{\text{liquid momentum flux}} \tag{1}$$

The operating conditions (see Table 1) are chosen to preserve the LOx mass flow rate (or equivalently the power) and keep J ratios roughly constant at the different pressure levels. At higher pressures, the velocity of the gaseous hydrogen decreases for a given mass flow rate. In order to maintain J, the outer diameter of the hydrogen annulus must decrease accordingly. However, at pressures above the critical pressure of oxygen (5.04 MPa), new operating points have been defined by keeping the values of the J ratio, further reducing the outer diameter but doubling the LOx

Table 1. Operating conditions of the Mascotte facility

Run condition	Pressure (MPa)	LOx mass flow (g s^{-1})	Gas mass flow (g s^{-1})	E	J
A	0.1	50	15.0	3.3	13.4
C	0.1	50	10.0	5.0	6.3
A-10	1.05	50	23.7	2.1	14.5
C-10	0.95	50	15.8	3.2	6.5
A-30	3	50	25.2	2.0	15.5
C-30	2.8	54	17.0	3.2	6.6
A-60	6.6	100	70.0	1.4	14.4
C-60	5.8	100	45.0	2.2	6.8
G1	4.68	43.9	101.2	0.43	
G2	5.59	44.4	143.1	0.31	

Points A and C correspond to LOx/GH_2 injection. Points G1 and G2 relate to LOx/GCH_4 operation. Liquid oxygen is injected at a temperature of 85 K. Gaseous hydrogen or gaseous methane are injected at temperatures of 288 K. E designates the oxygen to fuel mixture ratio. J stands for the gas to liquid momentum flux ratio.

mass flow rate. Trying to reach a pressure of 6.5 MPa in the combustor with a mass flow rate of 50 g s^{-1} of LOx is technically difficult because this would require a small nozzle throat that would have been difficult to cool properly.

More recently, the Mascotte rig was adapted to study LOx/CH_4 combustion (version V04). The most notable changes with respect to the previous versions concern the fuel feed line, which was modified to allow injection of either hydrogen or methane. The heat exchanger, placed on the feed system, is powerful enough to liquify the methane stream at a maximum mass flow rate $\dot{m}_{CH_4} = 250\,g\,s^{-1}$. This allows investigations of combustion conditions in which liquid methane is injected together with liquid oxygen. The flow rate of oxygen ranges from $\dot{m}_{LOx} = 20$ to$100\,g\,s^{-1}$. The combustion chamber is capable of withstanding pressures up to 10 MPa.

Operating conditions are presented in Table 1 for selected experiments at high pressure. In tests G1 and G2, methane is injected as a gas while the oxygen jet is subcritical (G1) or transcritical (G2). The mass flow rate of oxygen remains nearly constant at a value $\dot{m}_{LOx} = 45\,g\,s^{-1}$. Consequently, the heat release is around 0.55 MW for these two injection conditions if all the oxygen is consumed. The mixture ratio $E = \dot{m}_{LOx}/\dot{m}_{CH_4}$ is between 0.31 and 0.43, well below the mass stoichiometric value $s = 4$ characterizing the oxygen/methane reaction.

STRUCTURE OF HIGH-PRESSURE CRYOGENIC FLAMES

Observations of cryogenic combustion at low operating pressures (less than 1 MPa) have provided a wealth of information on the flame structure in the injector vicinity and in the farfield. It has been possible to examine effects of injection parameters and propose reasons for the observed changes in flame spreading. This has guided further experiments and numerical modelling efforts. Control parameters have been identified on this basis and physical descriptions of the flame structure have been proposed. This section discusses selected high pressure data and defines a physical description of the flame structure in the transcritical regime. The word transcritical is used here to designate the state of a fluid injected at a temperature which is lower than the critical value and at a pressure which exceeds the critical pressure.

Among the many parameters affecting the flame, it has become standard to consider the Reynolds numbers of each stream, the Weber

number of the liquid flow (when the pressure is below critical), the velocity ratio $V = v_{H_2}/v_{LOx}$, the injector diameter ratio d_{H_2}/d_{LOx}, the momentum flux ratio J defined by equation (1), the mixture ratio $E = \dot{m}_{LO_2}/\dot{m}_{H_2}$ and the operating pressure p or the ratio of the pressure to the critical pressure $\pi_c = p/p_{crit}$. A limited number of variables can be altered on a model scale test facility, such as injector geometry, exhaust nozzle throat diameter and mass flowrates. Consequently it is not possible to vary each parameter separately. Instead, it is necessary to study only parameters which are judged to be the most influential.

From previous engineering experience (see Gill, 1978) and from cold flow experiments and theoretical considerations, Hopfinger and Lasheras (1994), Rehab et al. (1997), Villermaux (1998), it was suggested that the momentum flux ratio, J, was the most influential parameter in determining the rupture of the central fluid in a coaxial jet, at least under subcritical conditions where break-up and atomization determine the liquid droplet sizes. This dimensionless group has served as the main scaling parameter in the experimental investigations carried out in the Mascotte test facility. Low-pressure-range experiments carried out with LOx/GH_2 propellants have confirmed that J controls the flame spread as shown by Herding et al. (1995, 1998) and Snyder et al. (1997). Initial hot fire tests were carried out in the low-pressure range up to 1 MPa ($\pi_{O_2} = p/p_c(O_2) = 0.2$). In this range, the oxygen stream behaves like a liquid jet, which is broken down into ligaments. These are subsequently atomized by aerodynamic shear stresses induced by the high speed hydrogen flow. When the chamber pressure is increased beyond 5.04 MPa (when $\pi_{O_2} > 1$), the oxygen jet passes from a subcritical to a supercritical state and its general structure is modified. Breakup and atomization prevailing at low pressure are replaced by a turbulent mixing process which determines the rate of transfer between dense oxygen at a temperature lower than the critical temperature and light oxygen at a temperature exceeding the critical value.

Other experiments have focused on the effect of inlet hydrogen temperature. This parameter affects the stabilization of the flame and the nearfield flow configuration. It was found that under cold-flow conditions some of the water vapor produced by the chemical reaction could condense to form an annular cloud surrounding the oxygen stream. At low injection temperatures the cloud was sufficiently dense to diffuse most of the light emitted by the flame, making visualization difficult (Juniper, 2001).

Table 2. Operating points of the cryogenic test facility (LO_x/GH_2 combustion)

	Previous work (VO1/VO2)	New results (VO3)
p (bar)	1, 5, 10	10, 70
J	Point C: $J = 6.3 \rightarrow 6.5$	Point C: $J = 3.0 \rightarrow 8.0$
	Point D′: $J = 9.8 \rightarrow 10.2$	
	Point A: $J = 13.4 \rightarrow 14.5$	Point A: $J = 9.0 \rightarrow 13.0$
Recess (d_{LOx})	0, 1	0, 1, 1.5
T_{H_2} (K)	298 K	298 K → 100 K

The operating conditions of hot fire tests are summarized in Table 2. Values of the momentum flux ratio J have been selected to change the quality of atomization (inadequate at low values of J, suitable at high values of this parameter). The value of J is the hardest to keep constant between tests because it depends on the ratio of the square of the velocities. The desired pressure is also difficult to achieve every time and there is some dispersion in the values of these parameters.

A large set of optical diagnostics has been used during the various test series including OH^* emission detection, backlighting, spectroscopy, planar laser light scattering and planar laser induced fluorescence of OH radicals (see Table 3, Brummund et al. (1995) for a review of optical diagnostics for cryogenic flames and Candel et al. (1998) for a synthesis of experiments in the low pressure range). The first three techniques were exploited in the high pressure range since fluorescence was thought to be inapplicable due to excessive quenching. However, recent experiments reported by Singla et al. (2005b) indicate that it is possible to obtain good quality fluorescence data at pressures as high as 6.3 MPa.

Structure of Transcritical LOx/GH_2 Flames

A selection of backlighting images is presented in Figure 3 (top). These show the dense oxygen jet and the regions containing steep refractive index gradients in the gas. The intensity of light defines the edge of the oxygen jet, which is taken to be the position where the intensity gradient changes most rapidly. Using this method, the oxygen jet position was found for all images in a sequence. These were then averaged to give a residence time along the line of sight. This yields a qualitative indication of the rate of expansion of the dense jet of oxygen.

Table 3. Experimental investigations of cryogenic combustion

	Laser-induced fluorescence OH, O_2	Emission imaging, Emission tomography	Backlighting, Light scattering	Combined imaging
Flame structure	Snyder et al. (1997) Candel et al. (1998) Cessou et al. (1998)	Herding et al. (1995) Herding et al. (1998) Mayer and Tamura (1996)	Herding et al. (1995) Mayer and Tamura (1996)	Snyder et al. (1997) Juniper et al. (2000)
Injection param.	Snyder et al. (1997)		Snyder et al. (1997) Mayer et al. (1996)	Snyder et al. (1997)
Effect of pressure	Singla et al. (2005b)	Juniper et al. (2000) Juniper et al. (2001b) Singla et al. (2005a)	Juniper et al. (2000) Juniper et al. (2001b) Mayer et al. (1998)	Juniper et al. (2001b) Singla et al. (2005a)
Flame stab.	Herding et al. (1996)		Mayer et al. (1998)	Mayer et al. (1998) Juniper et al. (2000) Singla et al. (2005a)
Effect of recess		Kendrick et al. (1998) Kendrick et al. (1999) Tripathi et al. (1999)	Juniper et al. (2001a) Juniper et al. (2005)	Juniper et al. (2001a)

The table only includes imaging studies.

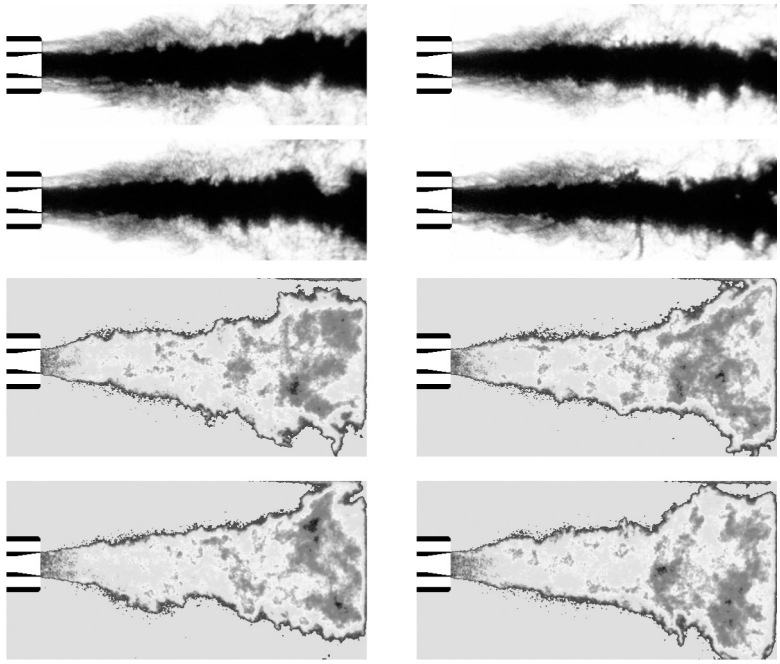

Figure 3. A sample of instantaneous backlighting images (top) and instantaneous OH^* images (bottom) for the broad field. The operating points and camera position are identical in both sets of images: Point C, $p = 7$ MPa (See Color Plate 4 at the end of this issue).

A selection of instantaneous OH^* emission images is shown in Figure 3 (bottom). These images, taken just after the backlighting images, correspond to exactly the same operating point and camera position. These images can also be averaged and processed with the Abel inversion (see Herding et al. (1998) for a presentation of this method and processing of low pressure flames and Juniper et al. (2000) for a discussion of its application in the high pressure range). The transformation yields the position of the average flame. These data may then be merged with the average oxygen jet position deduced from backlighting to form composite images as in Figure 4. (Note that in the top picture the average jet position near the injector was not available due to a partial icing of the visualization window close to the injection plane and corresponding screening of the light beam).

As in the low-pressure range, the flame begins at the injector, it spreads in the vicinity of the oxygen jet and does not penetrate into

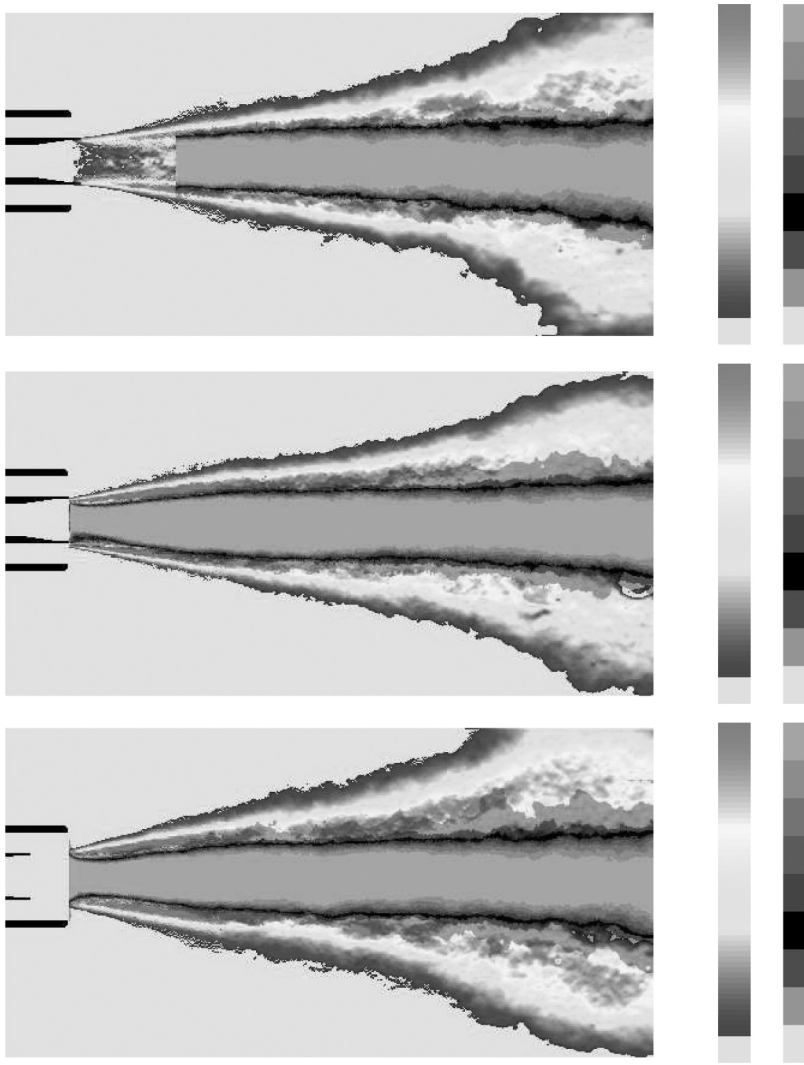

Figure 4. Combined emission and backlighting images. The colour scale corresponds to a slice of OH^* emission and the grayscale to the average jet position. Top: Point A, zero recess. Middle: Point C, zero recess. Bottom: Point C, recess of $1 \times d_{Lox}$ (See Color Plate 5 at the end of this issue).

the central core occupied by the dense stream of oxygen. In the high pressure range, the flame expansion angle is much smaller than that found in the low pressure experiments. It is also found that the

momentum flux ratio has less influence in this range. A detailed examination of the data gathered is carried out in Juniper et al. (2001b). A simplified model providing an interpretation of the spreading rates observed experimentally is given by Juniper et al. (2002). It is found that the low pressure flames are controlled by vaporization of droplets produced by the liquid jet breakup and subsequent atomization. The momentum flux ratio J determines the breakup process. In the high-pressure range, beyond the critical pressure of oxygen ($p > 5.05$ MPa), the flame spreading rate is controlled by turbulent mixing of the dense stream of oxygen with the lighter surroundings. The controlling mechanism is mass transfer from the dense jet to the lighter surrounding gas and this is mainly governed by the amount of interfacial surface between the dense and light fluids and by the local strain rates (see Jay et al., 2005, for a model accounting for these effects). Under these circumstances, the momentum flux ratio is less influential. The change in flame structure as pressure exceeds the critical pressure of oxygen is illustrated schematically in Figure 5. At low pressures, processes of atomization and vaporization control the rate of combustion and determine the flame length. At high

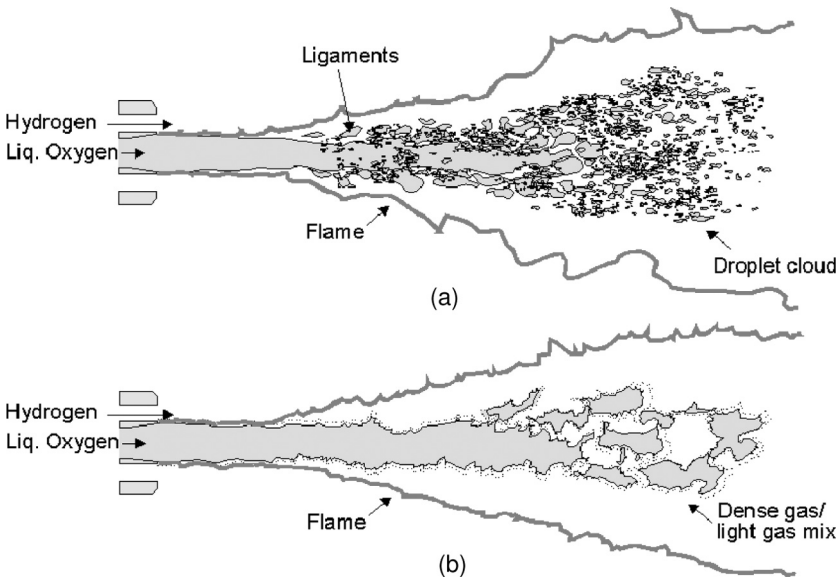

Figure 5. Schematic representation of subcritical (a) and supercritical (b) cryogenic jet flames.

pressures, mass transfer between the dense transcritical fluid and its surroundings is the rate controlling process.

Effect of Recess on Transcritical LOx/GH_2 Flames

It is known from many hot fire tests on complete engines that combustion efficiency is improved when the central injector is recessed inside the outer tube, as shown in Figure 1. Experiments carried out in the low pressure range ($p < p_c(O_2)$) indicate that recessing the LOx tube has a significant effect on flame spread (Kendrick et al., 1998, 1999). To explain these observations a one dimensional model of the internal flow is established in which the flame stabilized on the liquid oxygen injector lip, spreads inside the injector when the central tube is recessed. The flux of products formed by combustion inside the channel occupies part of the available area and, because of volumetric expansion, accelerates the outer gas flow. The momentum flux of the outer stream is augmented and this accelerates the liquid core breakup and improves its atomization thus augmenting the flame expansion rate. It has also been found in cold-flow experiments at low pressures, Strakey et al. (2002), that post biasing may be used to shift the liquid flux distribution away from the chamber wall.

There is some experimental evidence in the form of visualizations under hot fire conditions of the liquid oxygen stream indicating that recess also enhances long wavelength instabilities. This is illustrated in Figure 6, which displays backlighting images obtained from experiments on cryogenic injectors. The data correspond to injection at a pressure $p = 7$ MPa, MPa, exceeding the critical pressure of oxygen ($p_c(\mathrm{LOx}) = 5.04$ MPa). The dark region near the centerline corresponds to dense oxygen with a temperature lower than critical. This dense fluid is surrounded by oxygen gas at higher temperature. A flame, which is not visible in these images, separates the hydrogen stream from the oxygen stream. The ducted oxygen jet features large scale sinusoidal instabilities that are not present when the recess length is equal to zero. A detailed examination of backlighting images leads to the conclusion that recess favors the development of long wavelength instabilities. This is further supported by cold flow experiments (see Juniper et al., 2005) and by the instability analysis of Juniper and Candel (2003b). It is concluded that recess enhances a wake-like global instability in the central stream of a coaxial injector. The confined wake becomes globally unstable, while the flow in the absence of recess

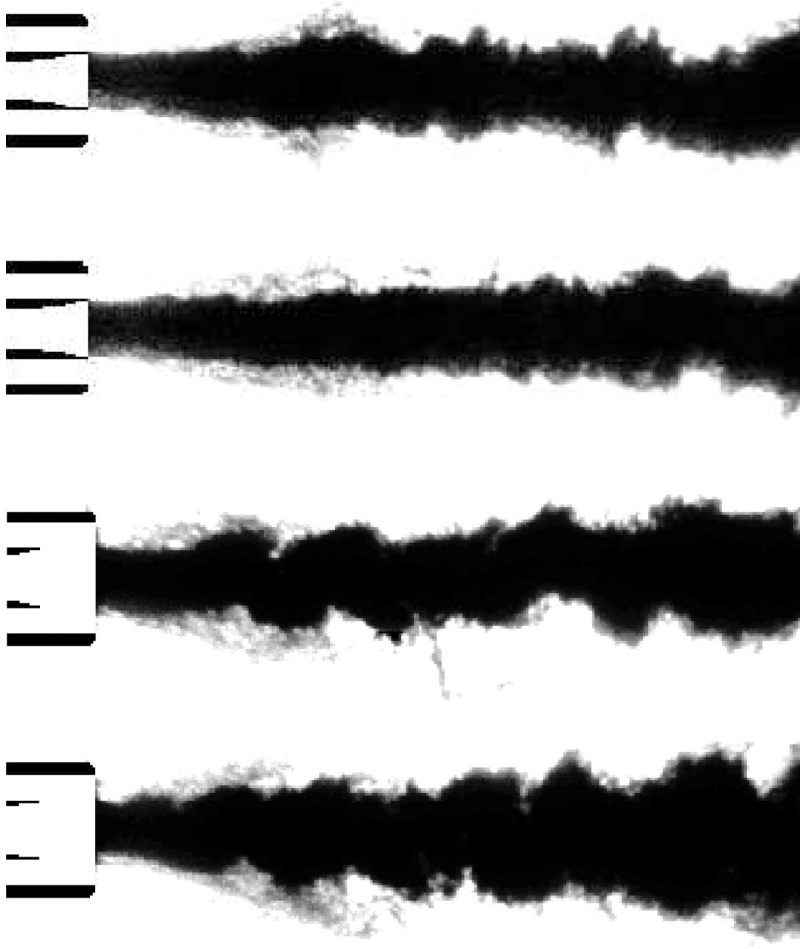

Figure 6. Effect of recess on the dense oxygen structure. Top two figures: Point C, zero recess. Bottom: Point C, recess of $1 \times d_{\mathrm{LOx}}$.

is only convectively unstable or marginally absolutely unstable. The global instability of the recessed flow aids rupture of the liquid jet and enhances mixing of the gas and liquid flows downstream.

FLAME STABILIZATION IN THE NEARFIELD

Flame spread in the nearfield is fundamental to flame holding. It is therefore important to focus on this region. This is accomplished by using the

same optical techniques combining emission and backlighting imaging (Juniper et al., 2001a). The backlighting setup is influenced by Schlieren effects because beam deviations are strong enough to deflect light out of the cone which is captured by the camera. Typical nearfield backlighting images obtained in the low and high pressure ranges are displayed in Figure 7.

The liquid oxygen jet appears as a dark black region in the two cases. The frontier of this jet is quite clear when the pressure is low and a thin interface separates the liquid from the gas. In the high-pressure situation, this frontier is fuzzy but still quite visible. The annular hydrogen stream is also distinguishable in both cases. When these images are averaged, the darkness of a pixel corresponds to the average time that a strong gradient has existed at that pixel's position. The strongest deviation occurs where gradients are perpendicular to the ray direction, which is in a slice through the jet's axis. Thus, to a first approximation, the images can be considered to be a slice of this plane and can be compared with the Abel-inverted emission images.

Instantaneous emission images obtained in the nearfield can be averaged and processed with the Abel inversion. They can then be superimposed on the average backlighting images, as shown in Figure 8. The flame edge is located in the near vicinity of the LOx injector and the flame then closely follows the dense oxygen boundary. Heat released by chemical conversion taking place near the dense oxygen stream induces a gradient of temperature and a steep change in oxygen density. The experimental data indicate that the flame is attached to the oxygen injector lip but that the anchor point is at a finite distance from the step. This is observed over the complete range of pressures, inlet velocities and hydrogen temperatures studied and illustrated in Figure 9, which shows the flame structure near the injection plane and a closeup of the vicinity of the LOx post lip. The flame edge is located just behind the lip at a small distance from this boundary. It is shown in a recent article by Juniper and Candel (2003c) and briefly summarized in the last section that the injector lip serves to stabilize the flame. Theoretical considerations and simulations of this region indicate that the most influential parameter is a nondimensional step height Ψ, which measures the size of the lip with respect to the flame thickness $\Psi = h_s/\delta_f$. When this parameter is large, the flame tucks behind the lip and is affected little by the Damköhler number. When this is small, the flame is thicker than the lip and it is exposed to the high speed hydrogen stream and becomes very

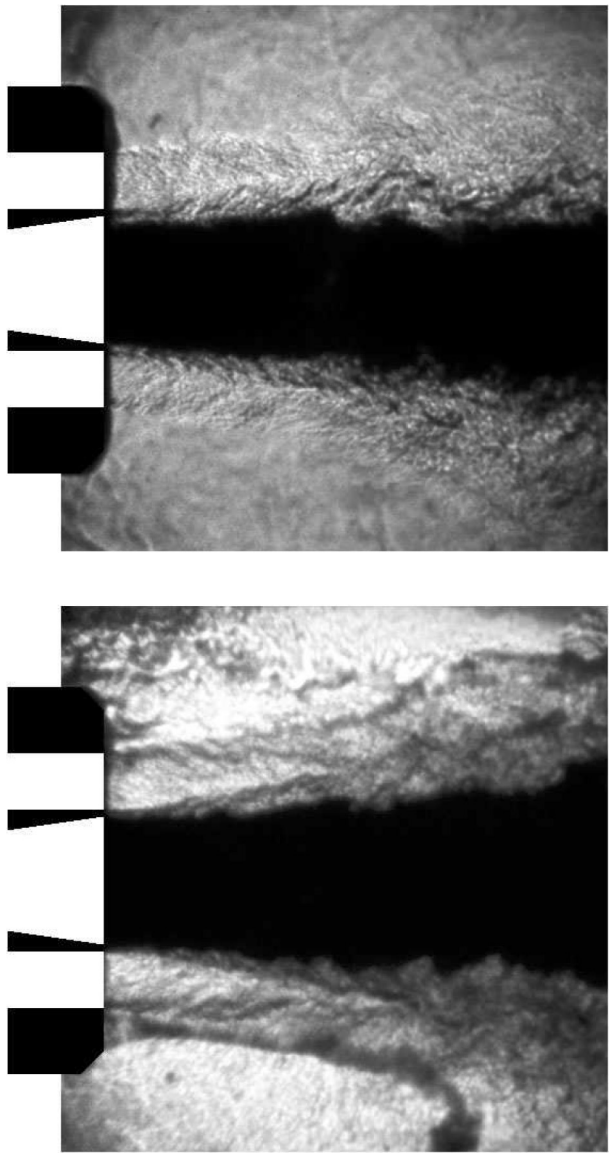

Figure 7. Instantaneous backlighting images obtained in the nearfield. Top, $p = 1$ MPa, zero recess. Bottom, point C, $p = 7$ MPa, zero recess.

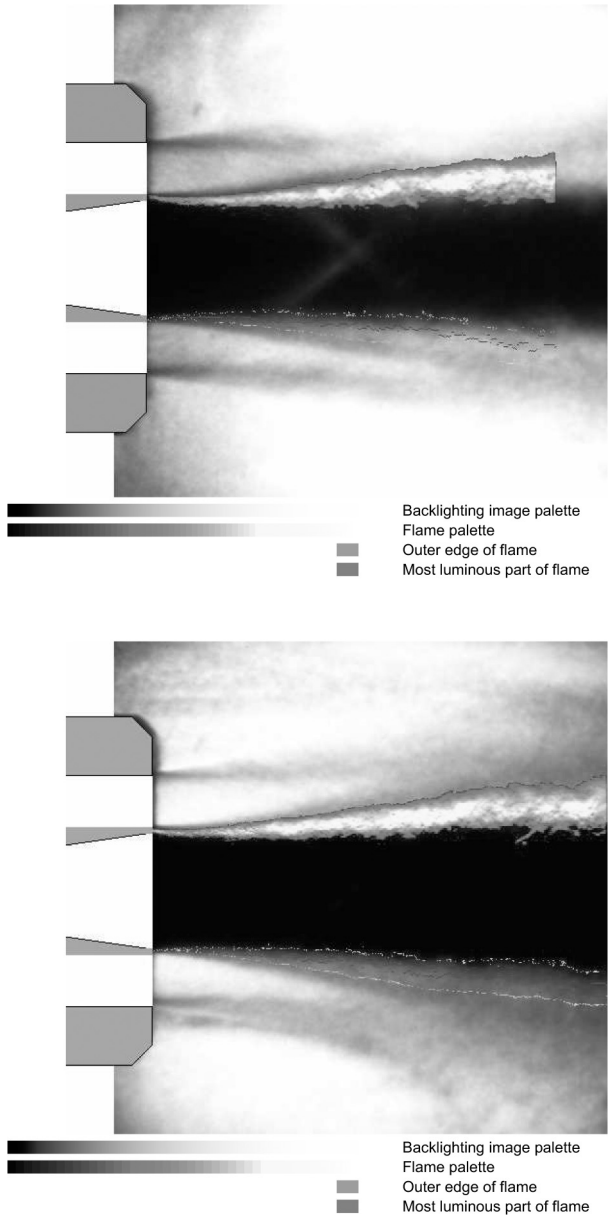

Figure 8. Combined emission and backlighting images. The colour scale corresponds to a slice of OH^* emission and the grayscale to the average backlighting image. Top, point A, $p = 7$ MPa, zero recess. Bottom point C, $p = 7$ MPa, zero recess (See Color Plate 6 at the end of this issue).

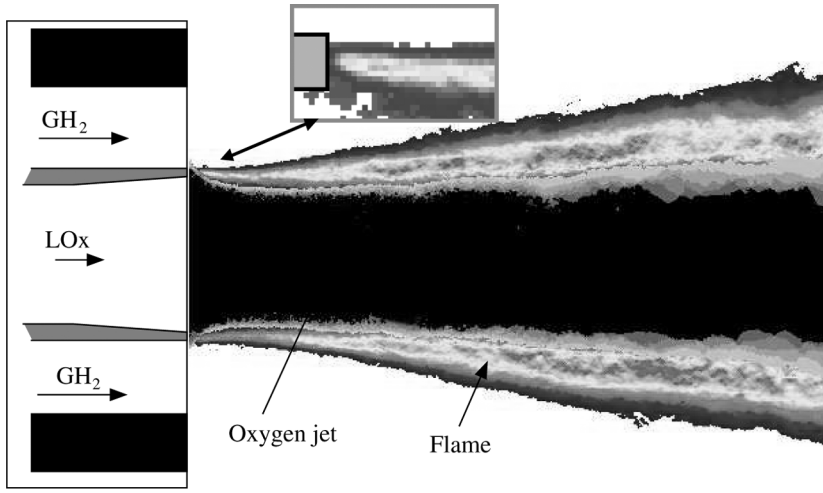

Figure 9. Combined emission and backlighting images. The colour scale corresponds to a slice of OH^* emission and the grayscale to the average backlighting image. Adapted from Juniper et al. (2000) (See Color Plate 7 at the end of this issue).

sensitive to the Damköhler number. Figure 9 corresponds to a case where $\Psi > 1$ and one expects that the flame will be well stabilized. More recent instantaneous images obtained by planar laser induced fluorescence of OH (Singla et al., 2005b) indicate that the anchor point is not fixed in space but moves around behind the oxygen lip. The spatial distribution of OH in the flame has a thickness which is comparable to the lip size. The flame is probably stabilized at other points around the circumference. It is also possible to consider that the lip size should be augmented by the thickness of the boundary layers established in the gas and liquid streams and that the stability criterion should be based on this augmented size: $\Psi = h_s^*/\delta_f$ where $h_s^* = h_s + \delta_{\mathrm{LOx}} + \delta_{GH_2}$.

INJECTION OF SUB- AND TRANSCRITICAL O_2/SUPERCRITICAL CH_4

Research on cryogenic combustion has mainly concerned liquid oxygen and gaseous hydrogen at various chamber pressures (0.1 to 7 MPa). There is, however, interest in the development of reusable liquid rocket engines operating with methane and oxygen as propellants. It is worth discussing fundamental information on the combustion process involving

this couple of propellants. One may envisage a situation in which both propellants are injected in a transcritical state and another set of conditions where oxygen is injected in a subcritical or transcritical state while methane is injected as a gas in a supercritical state. These various possibilities, explored by Singla et al. (2005a), indicate that the flame formed in the first situation differs significantly from the more standard cases involving one gaseous stream. This case will not be treated here and we only consider results corresponding to supercritical injection of methane and subcritical (G1) or transcritical (G2) injection of oxygen (Figure 10a, 10b). Injection conditions are gathered in Table 1. Figures 10a and 10b show Abel transforms of time average OH^* emission images. Nearfield images obtained from CH^* emission are also given in Singla et al. (2005a). The flame position with respect to the LOx jet

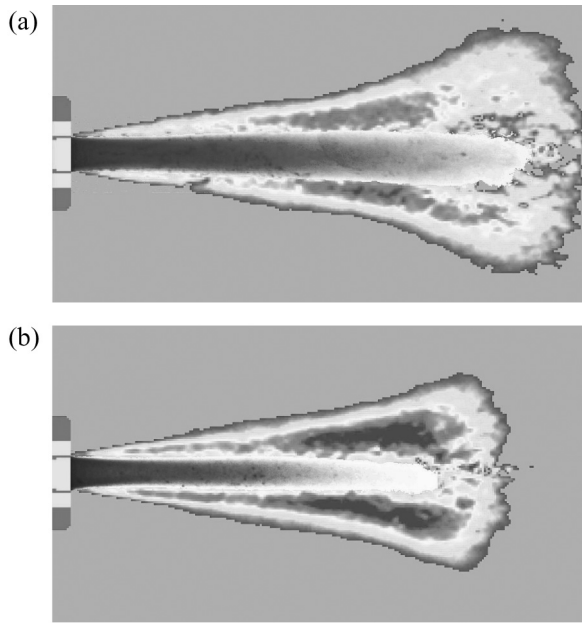

Figure 10. Liquid oxygen/gaseous methane combustion. Combined Abel transformed emission and backlighting images. The transformation is applied to average emission images obtained by summing 200 instantaneous images with exposure time 30 μs. The color scale corresponds to a slice of OH^* emission and the light to dark blue scale to the average jet position, (a) Point of operation G1, (b) Point of operation G2. From Singla et al. (2005a) (See Color Plate 8 at the end of this issue).

may be obtained by averaging images recorded with backlighting. The central jet appears as a dark region while the flame is shown on a color scale around the jet. Flame structures corresponding to LOx/GCH_4 injection are similar to those found in earlier studies on LOx/H_2 cryogenic flames. Light emission originates from an initially cylindrical envelope followed by an intense expanding zone. The reactive region closes abruptly before the end of the viewing window. There is a central zone corresponding to the oxygen jet devoid of luminosity, bounded by two narrow layers of light emission. The flame, stabilized on the lip of the injector, is wrapped around the oxygen jet.

At a reduced pressure $\pi_r(O_2) < 1$ (Figure 10a), the flame follows the surface of the cylindrical liquid jet for 5–6 d_{O_2} before blooming rapidly with an expansion angle α of about 20°. When the reduced pressure exceeds one, $\pi_r(O_2) > 1$ (Figure 10b), the flame expands more progressively up to 7 d_{O_2} where its blooming is less pronounced ($\alpha \simeq 10°$). The flame length (L_f) is shorter at $\pi_r(O_2) > 1 (L_f = 11 d_{O_2})$ than at $\pi_r(O_2) < 1$ where $(L_f = 14 d_{O_2})$. The time averaged emission intensity in the near injector region is greater when oxygen is injected in a transcritical state in the chamber (Figure 10). The reduction of the flame length is associated with a shorter oxygen jet. The length and thickness of the internal core diminish as the chamber pressure increases ($L_{O_2} = 7 d_{O_2}$ at $\pi_r(O_2) > 1$ while $L_{O_2} = 10 d_{O_2}$ at $\pi_r(O_2) < 1$) but the observed changes may be due in part to the augmented mass flow rate of methane, which induces a 40% increase in methane flow velocity. While the LOx/GH_2 and LOx/GCH_4 flames have many similarities, there are also some differences.

MODELLING OF FLAME EDGE AND FLAME SPREAD

The previous data may serve to guide and validate numerical modelling efforts. Substantial research is now being carried out to model the special features of high-pressure cryogenic combustion. This is reviewed comprehensively by Givler and Abraham (1996) and by Yang (2000). Much work has concerned elementary processes like mass transfer from and combustion of single droplets (Daou et al., 1995; Delplanque and Sirignano, 1993a, 1993b; Harstad and Bellan, 2001; Oefelein and Aggarwal, 2000) or supercritical mixing layers (Okong'o et al., 2002, Okong'o and Bellan, 2003). The evolution of jets and mixing layers under transcritical conditions is examined in this issue by Yang (2004). Calculations of cryogenic

flames have also been carried out in the classical RANS framework or with modern LES tools as in Oefelein and Yang (1998).

The stabilization mechanism of cryogenic flames is another topic of scientific and technical interest. It is known from experimental studies such as those described in the previous sections that the flame is stabilized in the wake of the oxygen injector lip and that it develops in the near vicinity of the oxygen flow. This is also observed in the simulations of Oefelein and Yang (1998). Under normal operating conditions, the flame is stable, the flame edge is close to the lip and the reaction front develops near the oxygen stream boundary. At some distance from the injection plane it becomes a highly turbulent brush. It is also known that below a critical hydrogen feed temperature, oscillations may develop at frequencies corresponding to the chamber's acoustic modes. Temperature seems to control the onset of this process, which suggests that the flame could lift off the oxygen injector making it more sensitive to acoustic coupling. With appropriate feedback this would lead to the observed oscillations; however, direct optical observations of this phenomenon are not available.

The mechanism that governs stabilization and the control parameters of this process are not well documented, even though they are essential in engineering analysis. Current practice relies on accumulated experience but a fundamental approach is needed (see Juniper and Candel, 2003c). It is first useful to imagine the different types of flame geometries as in Figure 11 and then use detailed calculations to identify configurations corresponding to stable flames and conditions leading to flame liftoff.

In these various schemes the flame base plays a central role. The analysis can be considered in two parts by distinguishing:

- A hot slow-moving zone just behind the oxygen injector lip in which the flow is laminar;
- A thin-spreading diffusion flame which becomes turbulent within a few millimetres.

Three mechanisms of flame blowout are possible.

1. A pilot flame remains shielded in the recirculation zone but the turbulent flame is extinguished just downstream in regions of excessive strain rate,

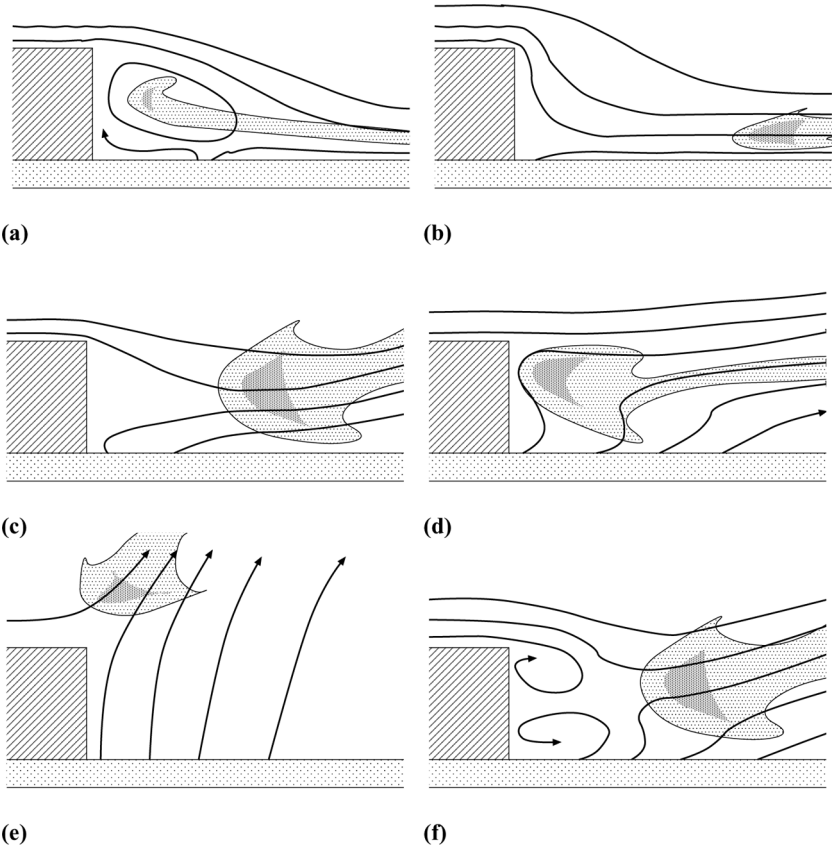

Figure 11. Various possible flow configurations of a flame behind a step over a liquid fuel, (a) The gaseous stream separates from the step and a flame starts in a recirculating zone, (b) The gaseous stream follows the step streamline. The flame tip is next to the liquid reactant. (c) Both streams meet half way behind the step, where a flame forms, (d) The gaseous stream separates from the step. Vaporized liquid reactant follows the streamline of the step. The flame forms at the top of the step, (e) The liquid reactant vaporizes rapidly. A corner flame forms above the step, (f) A double recirculation zone forms behind the step. The flame stabilizes downstream (from Juniper and Candel, 2003c).

2. The flame can no longer support itself in the recirculation zone,
3. Insufficient oxygen evaporates to feed the flame and it is quenched on the cold liquid surface.

The first blowout mechanism is explored in Juniper et al. (2003) by considering a counterflow hydrogen flame above condensed oxygen. It is shown that, at pressures of 1 bar and above, extinction by strain is impossible, even if the flame is pinched against the liquid oxygen surface. This reduces the study to the region just behind the lip of the oxygen injector.

The second and third extinction mechanisms are explored in Juniper and Candel (2003a) and Juniper and Candel (2003c) with particular reference to three nondimensional parameters, which are introduced in carefully planned stages. The first parameter is a Damköhler number affecting flame standoff distance in a cross-flow flame. This configuration is simple enough to permit theoretical analysis (see Mahalingam and Weidman, 2002). Another situation of interest is that of a flame above a liquid fuel. This introduces a new physical feature, vaporization, which requires another nondimensional parameter: the ratio of heat release due to chemical reaction to the liquid's latent heat of vaporization. The final parameter, the ratio of the LOx tube thickness to the flame

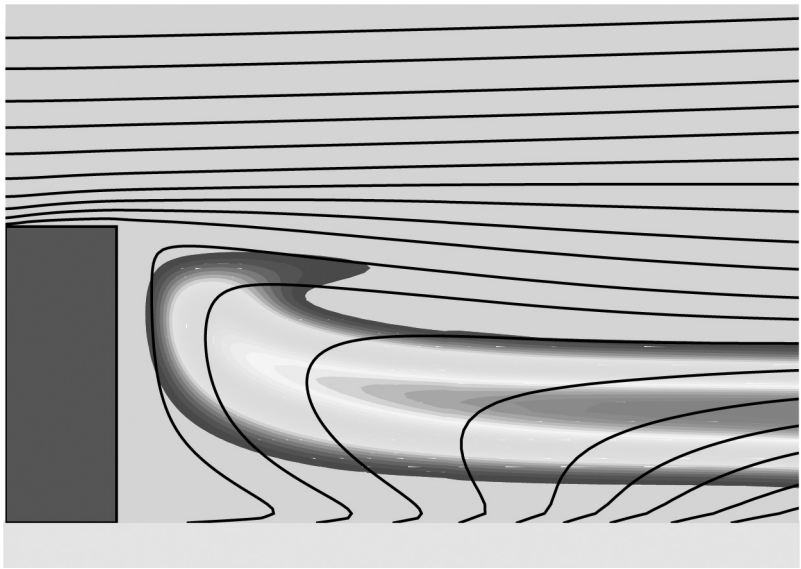

Figure 12. Hydrogen flame above condensed oxygen tucked behind a step of height 0.4 mm. The volumetric heat release is plotted on a color scale (max $= 1.2 \times 10^{11}$ J m^{-3} s^{-1}). Solid contours correspond to streamlines. $U_{H_2} = 190$ m s^{-1} $T_{H_2} = 350$ K, $T_{LOx} = 90$ K, $p = 0.1$ MPa (from Juniper and Candel, 2003c) (See Color Plate 9 at the end of this issue).

thickness $\Psi = h_s/\delta_f$ is introduced by Juniper and Candel (2003c). This is found to be the most influential parameter in the process of flame stabilization. For a thick LOx injector lip, one typically finds the flame structure

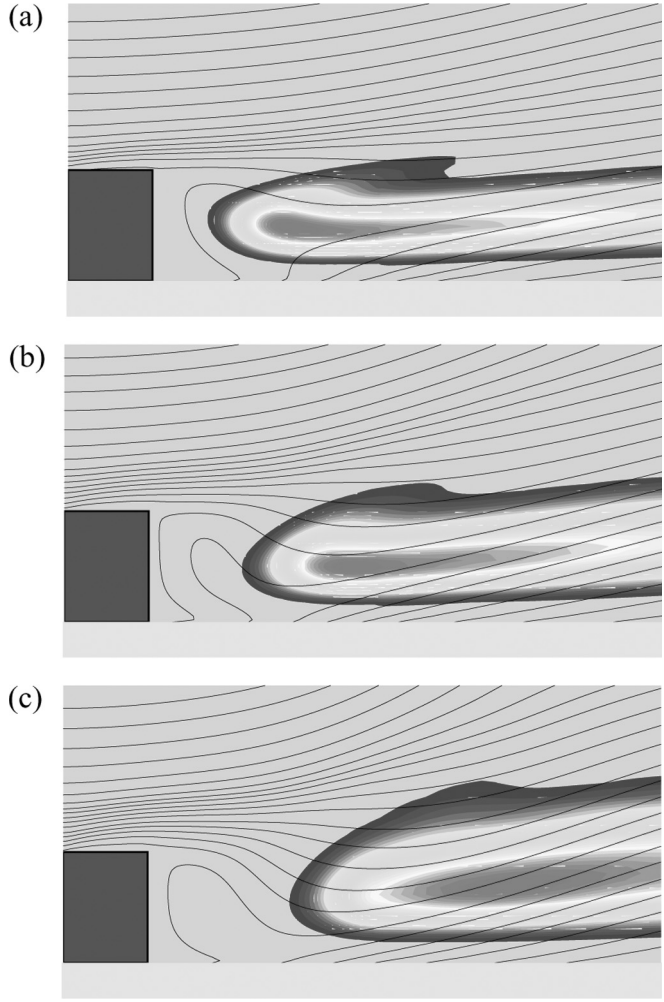

Figure 13. Flow configurations at different values of Ψ, which is the ratio of the step height, h_s, to the flame thickness, δ_f. For $\Psi > 1$ the flame tip is tucked into a slow-moving region behind the step. For $\Psi < 1$ the flame cannot support itself in this region. It becomes exposed to the free stream and blows off. (a) "Tucked flame," $h_s = 0.2$ mm, $\delta_f = 0.16$ mm, $\Psi = 1.25$. (b) "Borderline flame," $h_s = 0.2$ mm, $\delta_f = 0.21$ mm, $\Psi = 0.95$. (c) "Exposed flame," $h_s = 0.2$ mm, $\delta_f = 0.28$ mm, $\Psi = 0.71$. $U_{H_2} = 150\,\mathrm{m\,s^{-1}}$, $T_{H_2} = 350$ K (See Color Plate 10 at the end of this issue).

shown in Figure 12. The hydrogen stream separates from the edge of the step and the flame can tuck in the slow moving stream behind the step. The geometry is that of Figure 11(d). The configuration is similar to that of Oefelein and Yang (1998) and Deshpande et al. (1997). Results for a thinner lip $h_s = 0.20$ mm are shown in Figure 13. In all cases at this high value of U_{H_2}, the hydrogen stream separates from the edge of the step. There are two types of results, depending on Ψ. When the step exceeds the flame thickness, Figure 13(a), the flame can tuck into the slow-moving region behind the step. However, when the step size is smaller than the flame thickness, Figure 13(c), the flame is forced out of this zone. It then finds itself exposed to the main stream and is swept away. The latter type of solution is only stable for very low hydrogen velocities. The borderline case is obtained when the step height is equal to the flame thickness as shown in Figure 13(b).

The conclusions presented here are for H_2/O_2 flames at 1 bar but the same approach could be used at higher pressures to analyze flameholding. Because the analysis is carried out in terms of dimensionless groups, it should also be valid for other reactant combinations such as O_2/CH_4 and should provide a useful guideline for designing injectors.

CONCLUSIONS AND PERSPECTIVES

Research described in this article concerns cryogenic combustion in the high pressure range. Experiments carried out on the Mascotte facility cover a wide range of pressure (0.1 to 7 MPa). Some experiments were also carried out with LOx/methane injection. The gas to liquid momentum flux ratio ranges from 4 to 15 in the LOx/hydrogen flames and it is higher in the LOx/methane experiments. Emission and backlighting images obtained with two synchronized ICCD cameras provide a view of the LOx jet and the flame. The mean flame structure is extracted by taking the Abel transform of average emission images. This reveals the main features of the flame structure.

In the low-pressure range, below the critical pressure of oxygen (5.04 MPa) the flame burns in an external group combustion mode and takes the shape of a shell surrounding the LOx jet and LOx droplet cloud. This is well documented in previous studies. Detailed examination of the experimental results combined with simplified modelling indicates a change in behavior when the pressure exceeds the critical pressure of oxygen. Experimental and theoretical results indicate that the rate of

combustion is vaporization-limited when the pressure is below the critical pressure and is mixing-limited when the pressure is above the critical pressure. This suggests that, rather than improving atomization, one should attempt to increase mixing inside combustion chambers designed to operate above the critical pressure of the liquid reactant.

Experimental results also show that the flame remains attached to the lip of the oxygen injector over the complete range of pressure, inlet velocity and hydrogen temperatures studied. The stabilization mechanism has been elucidated by combining experimental information and detailed calculations of this small but important region of the flow. Research that has mainly concerned stable cryogenic flames formed by liquid oxygen and gaseous hydrogen now focuses on LOx/methane flames and on combustion dynamics and high frequency instabilities, a central problem in rocket propulsion. A program has been established by a French-German consortium formed by CNES, DLR, Snecma, EADS Astrium, Onera, and CNRS laboratories and a combination of experimental and computational investigations is underway.

REFERENCES

Barrère, M., Jaumotte, A., Fraeijs de Veubeke, B., and Vandenkerckhove, J. (1960) Rocket Propulsion, Elsevier, Amsterdam.

Brummund, U., Cessou, A., Oschwald, M.,Vogel, A., Grisch, F., Bouchardy, P., Pealat, M., Vingert, L., Habiballah, M., Snyder, R., Herding, G., Scouflaire, P., Rolon, C., and Candel, S. (1995) Laser diagnostics for cryogenic propellant combustion studies. *2nd International Symposium on Liquid Rocket Propulsion*, Chatillon, France, pp. 19.1–19.21.

Burick, R.J. (1972) Atomization and mixing characteristics of gas/liquid coaxial injector elements. *J. Spacecraft*, **9**, 326–331.

Burick, R.J. (1973) Optimum design of space storable gas/liquid coaxial injectors. *J. Spacecraft*, **10**, 663–670.

Candel, S., Herding, G., Snyder, R., Scouflaire, P., Rolon, C., Vingert, L., Habiballah, M., Grisch, F., Pealat, M., Bouchardy, P., Stepowsky, D., Cessou, A., and Colin, P. (1998) Experimental investigation of shear coaxial cryogenic jet flames. *J. Propul. Power*, **14**, 826–834.

Candel, S., Juniper, M., Scouflaire, P., Rolon, C., Clauss, W., Klimenko, D.N., Oschwald, M., Grisch, F., Bouchardy, P., and Vingert, L. (2003) Investigations of subcritical and transcritical cryogenic combustion using laser imaging and laser techniques. *5th International Space Propulsion Conference*, Chattanooga, Tennessee, CD Proceedings.

Cessou, A., Colin, P., and Stepowski, D. (1998) Statistical Investigation of the Turbulent Flame Geometrical Structures in a Liquid Oxygen/Gaseous Hydrogen Shear Coaxial Jet. *Proc. Combust. Instit.*, **27**, 1039–1046.

Daou, J., Haldenwang, P., and Nicoli, C. (1995) Supercritical burning of liquid oxygen (LOx) droplet with detailed chemistry. *Combust. Sci. Technol.*, **101**, 153–169.

Delplanque, J.P. and Sirignano, W.A. (1993a) Numerical study of the transient vaporization of an oxygen droplet at sub- and supercritical conditions. *Inter. J. Heat Mass Trans.*, **36**, 303–314.

Delplanque, J.P. and Sirignano, W.A. (1993b) Stability of transcritical LOx droplet vaporization in an idealized rocket combustor, AIAA Paper 93-0231. AIAA, Washington, D.C.

Deshpande, M., Venkateswaran, S., Foust, M., and Merkle, C. (1997) Finite splitter plate effects on flame holding in a confined hydrogen-oxygen shear layer, AIAA Paper 97-0258. AIAA, Washington, D.C.

Gill, G.S. (1978) A qualitative technique for concentric tube element optimization, utilizing the factor (dynamic head ratio-1), AIAA Paper 78-76. AIAA, Washington, D.C.

Givler, S.D. and Abraham, J. (1996) Supercritical droplet vaporization and combustion studies. *Prog. Energy Combust. Sci.*, **22**, 1–28.

Haarje, D.T. and Reardon, F.M. (1972) Liquid propellant rocket combustion instability, NASA SP 194, NASA, Washington, D.C.

Harstad, K. and Bellan, J. (2001) The d^2 variation for isolated LOX drops and polydisperse clusters in hydrogen at high temperature and pressures. *Combust. Flame*, **124**, 535–550.

Herding, G., Snyder, R., Rolon, C., and Candel, S. (1998) Investigation of cryogenic propellant flames using computerized tomography of OH emission images. *J. Propul. Power*, **13**, 146–151.

Herding, G., Snyder, R., Scouflaire, P., Rolon, C., and Candel, S. (1995) Emission and laser induced fluorescence imaging of cryogenic propellant combustion. *Conference on Propulsive Flows in Space Transportation Systems*, Bordeaux, France, pp. 1–14.

Herding, G., Snyder, R., Scouflaire, P., Rolon, C., and Candel, S. (1996) Flame stabilization in cryogenic propellant combustion. *Proc. Combust. Instit.*, **26**, 2041–2047.

Hopfinger, E. and Lasheras, J.C. (1994) Breakup of a water jet in high velocity co-flowing air. In Yule, A.J. and Dumouchel, C. (Eds.) *Proceedings of the 6th International Conference on Liquid Atomization*, Begell House, New York, pp. 110–117.

Jay, S., Lacas, F., and Candel, S. (2005) Combined surface density concepts for dense spray combustion. *Combust. Flame*, In Press.

Juniper, M. (2001) Structure et stabilisation des flammes cryotechniques, Doctoral thesis, Ecole Centrale Paris, Chatenay-Malabry.

Juniper, M. and Candel, S. (2003a) The effect of Damköhler number on the stand-off distance of cross-flow flames. *Combust. Theory Model.*, **7**, 563–577.

Juniper, M. and Candel, S. (2003b) The stability of ducted compound flows and consequences for the geometry of coaxial injectors. *J. Fluid Mech.*, **482**, 257–269.

Juniper, M. and Candel, S. (2003c) Stabilization of an edge diffusion flame behind a step over a liquid reactant. *J. Propul. Power*, **19**, 332–342.

Juniper, M., Darabiha, N., and Candel, S. (2003) The extinction limits of a hydrogen counterflow diffusion flame above liquid oxygen. *Combust. Flame*, **135**, 87–96.

Juniper, M., Leroux, B., Lacas, F., and Candel, S. (2005) Experimental determination of the instability mechanism in recessed coaxial injectors. *Experiments in Fluids, Submitted.*

Juniper, M., Tripathi, A., Leroux, B., Lacas, F., and Candel, S. (2001a) Stabilization of cryogenic flames and effect of recess. In *Combustion dans les moteurs fusées*, Cepadues Toulouse, pp. 222–231.

Juniper, M., Tripathi, A., Scouflaire, P., and Candel, S. (2002) Turbulent combustion of sprays under supercritical conditions. In Pollard, A. and Candel, S. (Eds.) *Turbulent Mixing and Combustion*, Kluwer, Dordrecht, pp. 439–446.

Juniper, M., Tripathi, A., Scouflaire, P., Rolon, C., and Candel, S. (2000) Structure of cryogenic flames at elevated pressures. *Proc. Combust. Instit.*, **28**, 1103–1109.

Juniper, M., Tripathi, A., Scouflaire, P., Rolon, C., and Candel, S. (2001b) The structure of cryogenic flames at subcritical and supercritical pressures. *Combustion dans les moteurs fusées*, Cepadues Toulouse, pp. 348–357.

Kendrick, D., Herding, G., Scouflaire, P., Rolon, C., and Candel, S. (1998) Effet du retrait sur la stabilisation des flammes cryotechniques. *Comptes Rendus de l' Académie des Sciences, Serie II b*, **326**, 111–116.

Kendrick, D., Herding, G., Scouflaire, P., Rolon, C., and Candel, S. (1999) Effects of a recess on cryogenic flame stabilization. *Combust. Flame*, **118**, 327–339.

Liang, P.Y., Fisher, S., and Chang, Y.M. (1985) Comprehensive modeling of a liquid rocket combustion chamber, AIAA Paper 85-0232.

Mahalingam, S. and Weidman, P. (2002) Activation energy asymptotic analysis and numerical modelling of a strained laminar corner flame. *Combust. Theory Modelling*, **6**, 155–172.

Mayer, W. and Tamura, H. (1996) Propellant injection in a liquid rocket oxygen/gaseous hydrogen rocket engine. *J. Propul. Power*, **12**, 1137–1147.

Mayer, W., Schik, A., Schaeffler, M., and Tamura, H. (2000) Injection and mixing processes in high pressure liquid oxygen/gaseous hydrogen rocket combustors. *J. Propul. Power*, **15**, 823–828.

Mayer, W., Schik, A., Schweitzer, C., and Schaffler, M. (1996) Injection and mixing processes in high pressure LOx/GH_2 rocket combustors, AIAA Paper 96-2620.

Mayer, W., Snick, A., Vielle, B., Chauveau, C., Gökalp, I., Talley, D., and Woodward, R. (1998) Atomization and breakup of cryogenic propellants under high-pressure subcritical and supercritical conditions. *J. Propul. Power*, **14**, 835–842.

Mayer, W.O.H., Ivancic, B., Schik, A., and Hornung, U. (2001) Propellant atomization and ignition phenomena in liquid oxygen/gaseous hydrogen rocket combustors. *J. Propul. Power*, **17**, 794–799.

Oefelein, J. and Aggarwal, S.K. (2000) Toward a unified high-pressure drop model for spray simulations. *Center for Turbulence Research Summer Program*, Stanford University, pp. 193–205.

Oefelein, J. and Yang, V. (1998) Modeling high-pressure mixing and combustion processes in liquid rocket engines. *J. Propul. Power*, **14**, 843–857.

Okong'o, N. and Bellan, J. (2003) Real-gas effects on mean flow and temporal stability of binary-species mixing layers. *AIAA J.*, **41**, 2429–2443.

Okong'o, N., Harstad, K., and Bellan, J. (2002) Direct numerical simulations of O_2/H_2 temporal mixing layers under supercritical conditions. *AIAA J.*, **40**, 914–926.

Pal, S., Moser, M.D., Ryan, H.M., Foust, M.J., and Santoro, R.J. (1996) Shear coaxial injector atomization phenomena for combusting and non combusting conditions. *Atomization Sprays*, **6**, 227–244.

Rehab, H., Villermaux, E., and Hopfinger, E. (1997) Flow regimes of large velocity ratio coaxial jets. *J. Fluid Mech.*, **345**, 357–381.

Singla, G., Scouflaire, P., Rolon, C., and Candel, S. (2005a) Transcritical oxygen/transcritical or supercritical methane combustion. *Proc. Combust. Instit.*, **30**, 2921–2928.

Singla, G., Scouflaire, P., Rolon, C., and Candel, S. (2005b) Planar laser induced fluorescence in high pressure LOx/GH_2 jet flames. *Combustion and Flame*, In press.

Snyder, R., Herding, G., Rolon, C., and Candel, S. (1997) Analysis of flame patterns in cryogenic propellant combustion. *Combust. Sci. Technol.*, **124**, 331–373.

Strakey, P.A., Talley, D., Tseng, L.K., and Miner, K.I. (2002) Effects of liquid-oxygen post biasing on SSME injector wall compatibility. *J. Propul. Power*, **18**, 240–246.

Tripathi, A. (2001) Structure des flammes cryotechniques a haute pression, Doctoral thesis, Ecole Centrale Paris, Chatenay-Malabry, France.

Tripathi, A., Juniper, M., Scouflaire, P., Rolon, C., Durox, D., and Candel, S. (1999) LOx tube recess in cryogenic flames investigated using OH and H_2O emission, AIAA Paper 99-2490. AIAA, Washington, D.C.

Villermaux, E. (1998) Mixing and spray formation in coaxial jets. *J. Propul. Power*, **14**, 807–817.

Yang, V. (2000) Modeling of supercritical vaporization, mixing, and combustion processes in liquid-fueled propulsion systems. *Proc. Combust. Instit.*, **28**, 925–942.

Yang, V. (2005) Fluid dynamic evolution of transcritical and supercritical cryogenic jets and mixing layers. *Combust. Sci. Technol.*, **177**, 2231–2265.

Yeralan, S., Pal, S., and Santoro, R.J. (2001) Experimental study of major species and temperature profiles of liquid oxygen/gaseous hydrogen rocket combustion. *J. Propul. Power*, **17**, 788–793.